ACS APPLIED MATERIALS & INTERFACES

Research Article

www.acsami.org

Notepad-like Triboelectric Generator for Efficiently Harvesting Low-Velocity Motion Energy by Interconversion between Kinetic Energy and Elastic Potential Energy

Guanlin Liu, Qiang Leng, Jiawei Lian, Hengyu Guo, Xi Yi, and Chenguo Hu*

Department of Applied Physics, Chongqing University, Chongqing 400044, P.R. China

Supporting Information

ABSTRACT: Great attention has been paid to nanogenerators that harvest energy from ambient environments lately. In order to give considerable output current, most nanogenerators require high-velocity motion that in most cases can hardly be provided in our daily life. Here we report a notepad-like triboelectric generator (NTEG), which uses simple notepad-like structure to generate elastic deformation so as to turn a low-velocity kinetic energy into high-velocity kinetic energy through the conversion of elastic potential energy. Therefore, the NTEG can achieve high current output under low-velocity motion, which completely distinguishes it from tribogenerators previously reported. The factors that may affect the output performance are explored, including the number of slices, active length of slice, press speed, and vertical displacement. In addition, the working mechanism is systematically studied, indicating that the efficiency of the generator can be greatly enhanced by interconversion between kinetic energy and elastic potential energy. The short-circuit current, the open-circuit voltage, and power density are 205 μA and 470 V and 9.86 W/m^2, respectively, which is powerful enough to light up hundreds of light-emitting diodes (LEDs) and charge a commercial capacitor. Besides, NTEGs have been successfully applied to a self-powered door monitor.

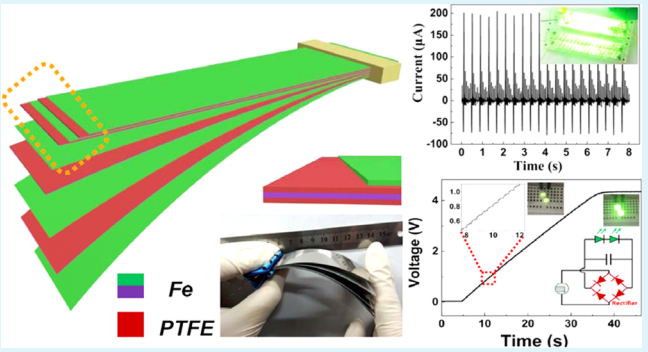

KEYWORDS: *triboelectric generator, notepad-like structure, self power, door monitor, elastic deformation*

1. INTRODUCTION

Since the concept of nanogenerators was first proposed in 2006,[1] it has been drawing attention from all over the world because of its great potential for harvesting the energy from ambient environments to provide power for small devices and build self-powered systems.[2,3] Therefore, more and more researchers are devoting their time and energy to this field. Generally, different types of generators are built based on the piezoelectric effect,[4−6] pyroelectric effect,[7−9] and triboelectric effect,[10−12] of which, the generator based on triboelectric effect is most favored due to its high efficiency, easy fabrication, and low cost. With the use of a triboelectric generator (TENG), many kinds of mechanical energy have been successfully collected from daily motion like airflow,[13,14] waterflow,[15,16] vibration,[17,18] sliding,[19,20] and rotation[21−23] and from energy like sound[24] and biological energy.[25,26] Therefore, we could see that TENG is a sort of efficient, cost-effective, and promising device to harvesting energy from ambient environments.

However, in order to make generators produce considerable current output high-velocity motion or large amplitude motion is required in most cases. Apparently, usual daily motion like the opening of doors, the rotating of taps, and the sliding of drawers could never provide that high speed and persistence of motion, which can not generate effective output and thus limits the application of triboelectric generators. So, it is a great challenge for us to improve the TENG so as to make it widely applicable in our daily life.

In this paper, we innovatively design a NTEG based on the motion of spring lamination. The notepad-like spring lamination of the NTEG is used as an energy storage and conversion device, in which, the kinetic energy of low speed motion is first transformed into elastic potential energy through elastic deformation stored in the device, and then the elastic potential energy released is to be transformed into the kinetic energy of high speed motion. Thus, high output current is obtained. Moreover, the unique flexible notepad-like structure could not only effectively realize the conversion of low speed motion to high speed motion but also broaden the application of the TENG greatly. However low the speed is, the TENG can be used to collect energy from sources such as vibration, sliding, and rotation. The working mechanism and performance in different conditions are elaborately illustrated. The maximum output current, open-circuit voltage, and power density are obtained as much as 205 μA, 470 V, and 9.68 W/m^2,

Received: October 27, 2014
Accepted: December 22, 2014
Published: January 7, 2015

DOI: 10.1021/am507477y
ACS Appl. Mater. Interfaces 2015, 7, 1275−1283

respectively. Besides, the NTEG can be used to light up hundreds of LEDs and to charge commercial capacitors successfully, and it can also be applied to a self-powered door monitor, which could monitor the door from a distance. The NTEG has great potential in smart home sensing, medical infrastructure/environmental monitoring, defense technology, and personal electronics. It presents a great progress in the structure design of the nanogenerator for its practical applications.

2. EXPERIMENTAL SECTION

2.1. Fabrication of Notepad-liked Triboelectric Generator (NTEG). Figure 1a illustrates the structure of NTEG, which is composed of stacked steel slices fixed on one end and free on the other end. At the fixed end, 2 cm is spared to attach copper wires and are gripped by a clamp. The slices are in different lengths and form steps at the free end to make sure that the slices can be separated effectively when a force is applied on the end. The enlarged view of the slices is shown in Figure 1b, which illustrates that the spring laminations are made up of bare metal slices and the metal slices covered with PTFE on their surfaces. The two kinds of slices are alternately stacked together. All the bare metal slices are connected together to form a M electrode. The metal slices covered with PTFE are connected by copper wires to form a P electrode. Both top and bottom slices are M electrodes, as shown in Figure 1a and c.

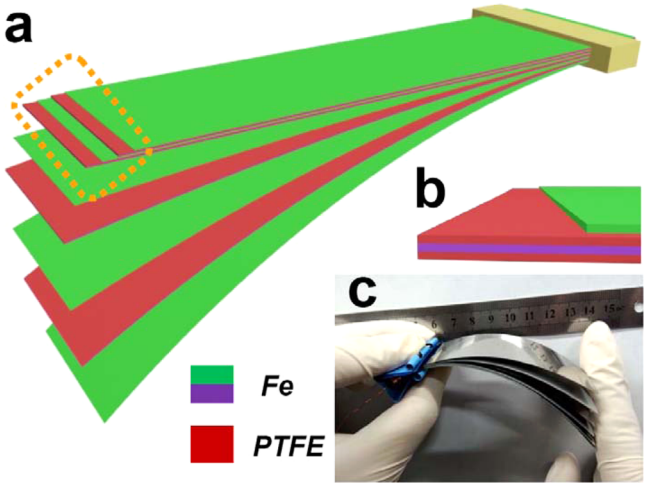

Figure 1. (a) Schematic diagram of the notepad-like triboelectric generator (NTEG) and (b) enlarged view of the red dotted part. (c) Digital photograph of the NTEG.

M Electrode. An M electrode is composed of exposed metal slices. In this experiment, the metal slices are made of spring steel, which has good flatness, good elasticity, a well polished surface, and fatigue-resistance. We cut the commercial metal slice (width 25 mm, length 5000 mm, thickness 0.08 mm) into lengths (94, 98, 102, and 106 mm), and then after ethanol spray treatment and being dried at 40 °C, we connect those slices together with copper wires, of which, one is taken out as the electrode.

P Electrode. We cut the slices into lengths (96, 100, and 104 mm). After ethanol spray treatment and being dried at 40 °C, each metal slice is covered on both faces with commercial PTFE (thickness 0.1 mm) as electrets using double-sided adhesive (thickness 0.1 mm). All the wires are covered with insulated layer to prevent short circuiting.

2.2. Characterization of NTEG. The output performance of the NTEG is measured using a Stanford low-noise current preamplifier (Model I SR570) and a Data Acquisition Card (NI PCI-6259). Figure S1 schematically shows the measuring system. In the experiment, we use iron support and clamp to hold the NTEG horizontally. A fan blade fixed on a rotating motor (51K40RA-G) hits the slices periodically at different rotating speeds that produces different hitting frequency (Figure S1). The length between A and B is active length l (Figure 2a and Figure S2). The distance between the acting point of the blade and the end of the shortest metal slice is defined as the hitting position H (Figure S2), which affects the vertical displacement x.

3. RESULTS AND DISCUSSION

3.1. Working Mechanism of NTEG. Electret PTFE film could hold charges (charge densities up to 5×10^{-4} C/m^2 with a theoretical lifetime of hundreds of years).[27] The electricity of the TENG originates from the mechanical motion based on triboelectrification and electrostatic induction: the periodic contact and separation between two different medium with opposite charges change the induced potential difference across the two electrodes and thereby drive the alternating flow of electrons through an external load.[10,28−30] Figure 2 demonstrates the electricity generation process in details. Before experiment, the NTEGs have been hit for several times; therefore, the rubbed electret PTFE holds negative bound charges and the neighboring electrodes with the same quantity of positive charges. After being bent down by vertical press (Figure 2a), the slices harvest the mechanical work and then store it as elastic potential energy. At this stage, no current output is observed. As shown in Figure 2, the left or right arrow of the ampere meter stands for the current and its direction. When the arrow points upward, it means that there is no current. When the first slice of M electrode is released, the potential difference generated around the PTFE forces the positive charges on the M electrode to flow to P electrode through the external circuit (Figure 2b). That means the free electrons flow to M electrode from P electrode, and thus reverse current is generated. When the second slice of the P electrode is released (Figure 2c), the positive charges on the third slice flow to P electrode to offset the potential difference through the external circuit. Then the second released slice (P electrode) bounces abruptly and hits the first slice (M electrode) forcefully at a high speed. Thereby, positive charges are induced in the M electrode very quickly (Figure 2d) and free electrons flow from the M electrode to P electrode, generating a high pulse current. When the third slice is released (Figure 2e), the positive charges in the M electrode flow to the P electrode. Then the third released slice (M electrode) hits the second slice (P electrode) (Figure 2f), meanwhile, forward pulse current is generated. The subsequent process of release and hit goes the same as before until the last slice of M electrode. As there is no PTFE below it when the last slice is released, no reverse current is generated at the moment the last slice is released (Figure 2g). Subsequently, when the last slice hits the second last slice, high output current is generated just like before. Figure 2h shows the wave pattern of NTEG output current when the device of seven slices is pressed at lower speed where the current at a−g points corresponds to the each state in Figure 2a−g. The wave pattern illustrates that NTEG could produce numbers of pulse current as big as 44 μA when the speed is slow. Therefore, we could see that NTEG has a great potential to generate high output current under low speed motion, indicating the electromechanical conversion efficiency is greatly enhanced.

The alternate current in the external circuit is caused by the alternately separation and contact of M and P electrodes. The value of the transferred charges of every separation and contact could be given by formula 1:

DOI: 10.1021/am507477y
ACS Appl. Mater. Interfaces 2015, 7, 1275−1283

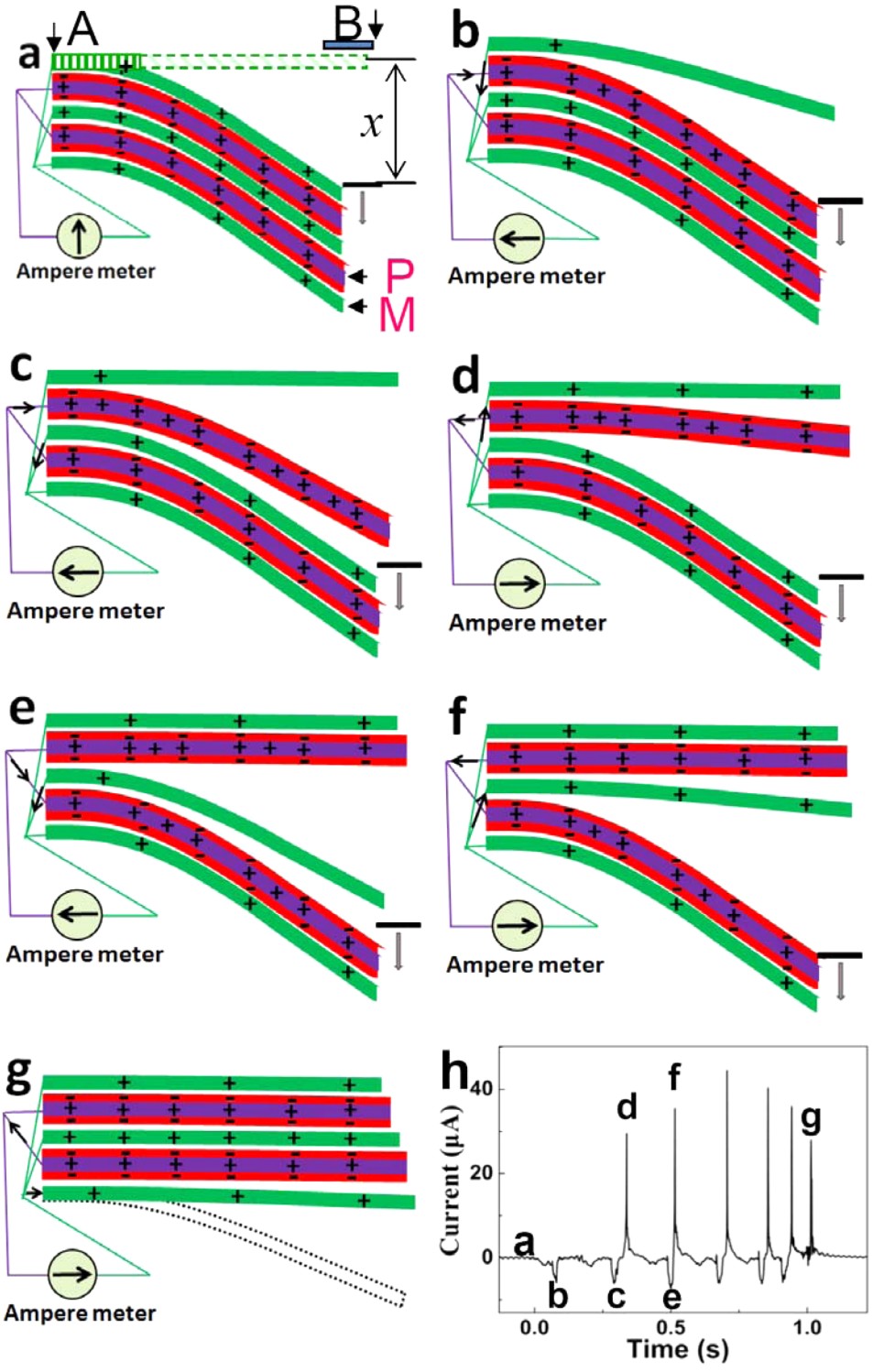

Figure 2. Working principle of the NTEG. (a–g) Schematic diagrams of the charge distributions and current direction when the slices move in one period. (h) Current–time plot corresponding to the a–g process.

$$Q = \alpha\sigma la \tag{1}$$

The generated current could be given by formula 2:

$$I = \frac{\Delta Q}{\Delta t} = \frac{\alpha\sigma la}{d/v} = \frac{\alpha v\sigma la}{d} \tag{2}$$

where σ, l, and a, respectively, represent the surface triboelectric charge density, the average active length of spring slices, and the width of the slices (25 mm). The coefficient α in formula 1 represents the ratio of the actual working length L to the average active length $\alpha = L/l$, which is related to the separation of slices near the fixed end (Figure S2). To simplify the charge induction process of separation and contact, two approximations are used. One is that the slices are separated and contacted in parallel mode when they are in a small gap. The other one is that the effective range of the charge induction is a constant of d (Figure S2). Thus, we get formula 2, where v

DOI: 10.1021/am507477y
ACS Appl. Mater. Interfaces 2015, 7, 1275–1283

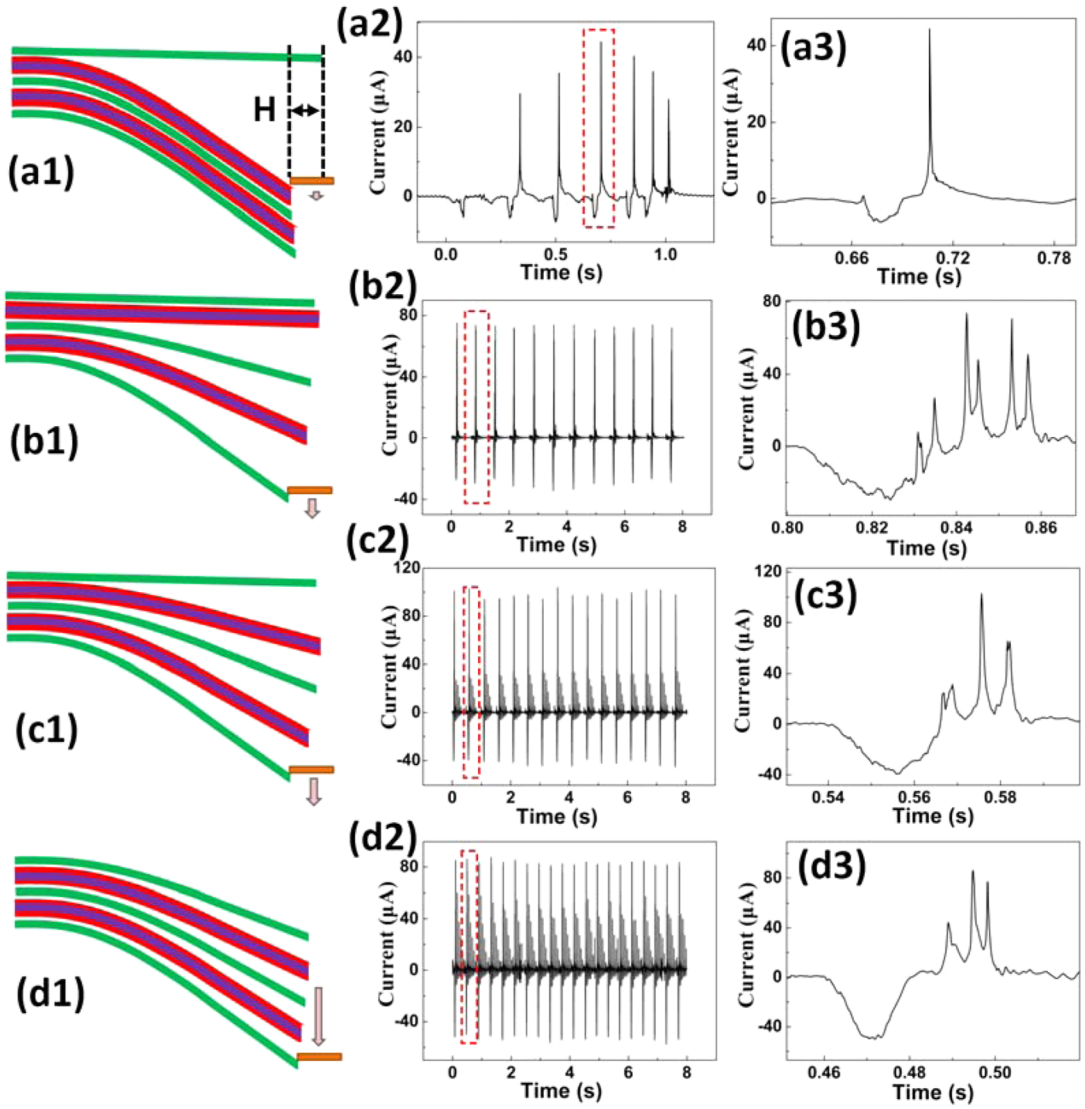

Figure 3. Possible four states of NTEG. (a1−d1) Structure diagrams of the four states. (a2−d2) Corresponding output current of the four states. (a3−d3) Corresponding enlarged output current of the four states in marked squares.

represents the relative speed of two slices separating and contacting. The reason why the forward current is much higher than that of reverse current is that the relative speed of contact is faster than that of separation. When the lower slice contacts the upper slice, the speed of the lower slice generated from the kinetic energy which is converted from large elastic potential energy is relatively high.

3.2. Factors that Influence Output Performance. *3.2.1. Hitting Speed.* It could be observed that when the blade hits the NTEG, there exist four situations, as shown in Figure 3: (A) When the blade moves very slowly, each slice could be well separated in turn and the current wavebands generated by the slices would not affect each other (a1−a3). (B) When the blade moves a little faster, the moment one slice is released, the slices that are released before it are still bouncing to the balanced position (b1). From the enlarged plot of current−time in unit period (b2 and b3), we can observe that the superposition of some reverse currents generated by the initial separation that are not affected by the collisions of subsequent released slices increases the reverse current output. On the one hand, due to the superposition of the forward current generated by the collisions of the slices released before and the reverse current generated by the separation of the subsequent released slices, the peaks of a few initial forward current pulses are decreased. On the other hand, the superposition of forward current generated by the collisions of the last a few released slices increases forward current pulses (b3) which are not affected by the reverse current generated by separation. (C) When the speed of the blade keeps increasing and then reaches a point, a critical state will emerge. When the last slice is released, the first released slice just arrives at balanced position. In this case, all the slices separate each other to a maximum degree (c1). After the last slice is released, because the releases and the collisions go separately, the forward currents superimpose the forward currents, and similarly, the reverse currents superimpose the reverse ones (c2 and c3). Thus, theoretically, we have the biggest output. We call this process optimal separation state. (D) On the basis of optimal separation state, we further increase the speed of the blade. Under this circumstance, when the last slice is released, the first released slice has not reached the balanced position yet, which makes the slices of electrodes much too dense (d1). Even though output pulse currents are further superimposed, the near fixed side of the electrodes could not separate

DOI: 10.1021/am507477y
ACS Appl. Mater. Interfaces 2015, 7, 1275−1283

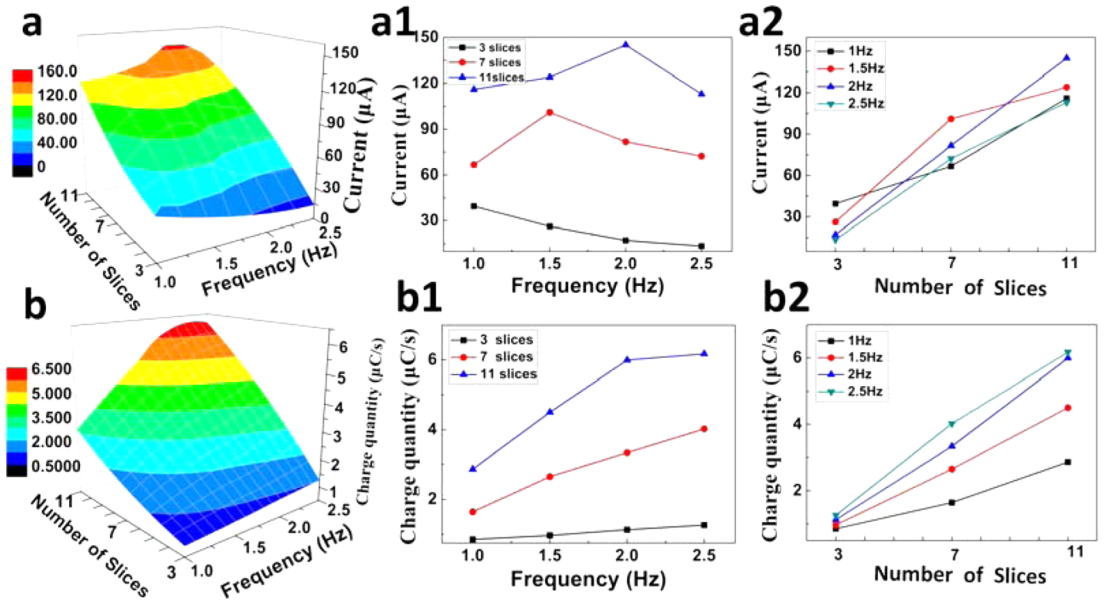

Figure 4. Performance of the NTEG. (a) 3D surface graph of the varied output current on changing both the number of slices and frequency. (a1 and a2) Corresponding 2D graphs derived from the 3D surface graph. (b) 3D surface graph of the varied charge quantity on changing both the number of slices and frequency. (b1 and b2) Corresponding 2D graphs derived from the 3D surface graph.

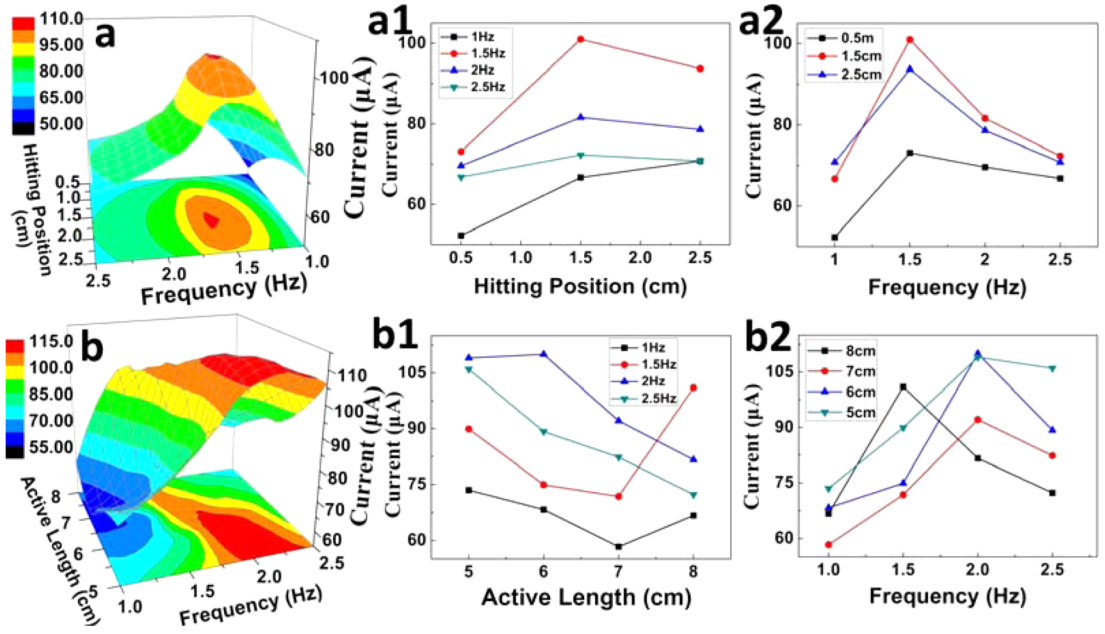

Figure 5. Performance of the NTEG. (a) 3D surface graph of the varied output current on changing both the hitting position and frequency. (a1 and a2) Corresponding 2D graphs derived from the 3D surface graph. (b) 3D surface graph of the varied charge quantity on changing both the active length and frequency. (b1 and b2) Corresponding 2D graphs derived from the 3D surface graph.

effectively, and the actual working length L becomes shorter, which means that α is smaller. And according to formula 1, the value of transferred charges becomes smaller in unit period. Therefore, much too fast hitting speed on the slices is not good for the increase of output (d2 and d3). In conclusion, the speed of the blade affects the output greatly. It is of great importance to take a deep research into how the hitting frequency on the slices influences the output. Besides, we find that the stronger oscillated waveform emerges before the main waveform as the frequency increases, which is caused by the blade hitting. Therefore, the stronger oscillated waveform is attributed to the higher hitting frequency. And later the gradually diminishing oscillating current is caused by residual oscillation, which increases the output and the value of transferred charges in unit period. Since all the slices leave the equilibrium position in a gradually reduced velocity and return the equilibrium position in a high velocity during the residual oscillation, the forward current pulses are much higher than those of the backward currents (Figure S3).

3.2.2. Number of Slices. The number of slices determines the number of pulse currents and the quantity of the transferred charges in one period, and it also indirectly affects the peak value of the output currents. Therefore, slice numbers of 3, 7, and 11 have been fabricated for the NTEG to test the output

DOI: 10.1021/am507477y
ACS Appl. Mater. Interfaces 2015, 7, 1275−1283

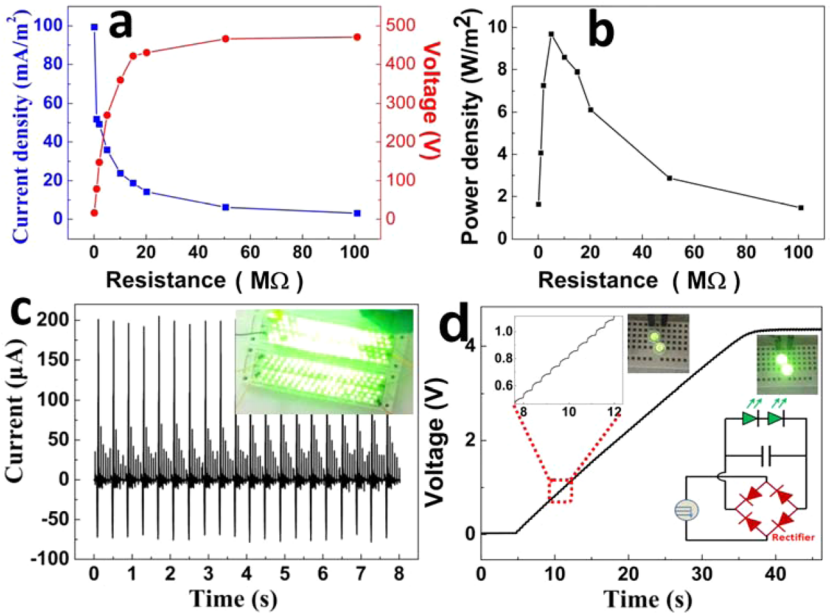

Figure 6. (a) Output current and voltage and (b) the output power under different external loads. (c) Output current of the 11-slice NTEG. (inset) Photography of driving LEDs using this NTEG. (d) Voltage curve of the capacitor charged by the NTEG. The left up-corner and the right bottom-corner insets give enlarged plots during charging and the equivalent circuit for charging and lighting the LEDs. The other two insets exhibit the photographs of the lit LEDs during the charging.

performance at different frequencies. The results are shown in Figure 4, where the 3D graphs are all smoothened by bilinear difference arithmetic (Figure 4a and b). Four 2D graphs derived from these two 3D graphs by projecting are depicted in Figure 4a1, a2, b1, and b2, revealing the output current and the quantity of the transferred charges in unit time at different frequencies and with different slice numbers, respectively. As shown in Figure 4a–a2, by increasing the number of the slices, performance can be greatly improved. However, the frequency for the NTEG with different slice numbers to reach the respective optimum output state is different, and the larger the slice number, the higher the frequency needed. Thus, it is verified that the maximum output performance is reached in the state of optimal separation of slices (Figure 3c). The time for the first slice to return to the equilibrium position is nearly the same for the different number of slices. In order to reach the state of optimal separation, all electrodes have to be released just as the first slice returns to the equilibrium position; therefore, the faster blade speed is required (higher frequency). Besides, at frequencies of 1, 1.5, and 2 Hz, respectively, the short-circuit currents of NTEGs with electrodes of 3, 7, and 11 reach their maximum values of 39.5, 101, and 145 μA, respectively. As shown in Figure 4b–b2, with the increased slice numbers and frequencies, the transferred charges in unit time increases linearly. The same result appears by shortening the actual active length (Figure S4).

3.2.3. Hitting Position. The influence of the hitting position H (Figures 3a and S2) and the active length l of the NTEG with seven slices on its output performance are shown in Figure 5. To better illustrate the shaded part, the contour map is added to the X–Y plane. Four 2D graphs derived from these two 3D graphs (Figure 5a and b) by projecting are depicted in Figure 5a1, a2, b1, and b2, revealing the output current with different H and active lengths, respectively. As shown in Figure 5a–a2, with increase in H (increase in pressed displacement x) and frequency, the output current increases at the beginning and then decreases. Besides, the maximum values occur at H= 1.5 cm and at the frequency of 1.5 Hz respectively in most cases. Thus, the later experiments are all conducted at H = 1.5 cm.

Obviously, the slices move faster at larger press displacement x after they are released. Consequently, both too larger x and hitting frequency would result in overtense of the slices to reduce the output as shown in Figure 5a–a2. Furthermore, we have carried out tests for NTEGs with 3 and 11 slices, and the results have further verified our theory (Figure S5).

3.2.4. Active Length. Figure 5b–b2 show the experimental data obtained by the comparative experiments of changing the active length of the seven-slice NTEG. As shown in Figure 5b, the output current decreases as active length increases from 5 to 7 cm at frequency of 1 Hz, indicating that shorter slices get a higher speed after being released from the same press displacement. However, such increase of output by shortening the active length is only in a small range as too short slice will greatly reduce the working area. On the other hand, the output current first decreases and then increases with an increase in active length at low frequency, while at high frequency, it decreases monotonically with an increase in length. The slices with different active lengths reach the respective optimum output state at different frequencies. With the larger number of slices, the optimal separation state appears at higher hitting frequency, which is demonstrated by the measurement on 3-slice, 7-slice, and 11-slice NTEGs, as shown in Figure S6.

3.2.5. External Loads of NTEGs. It is indispensable to investigate the actual output power in order to check the efficiency of the NTEG. Resistors are used as external loads. As shown in Figure 6, for the 11-slice NTEG with an active length of 6 cm at frequency of 2.5 Hz and the hitting position of 1.5 cm, the short-circuit current and open-circuit voltage reach 205 μA and 470 V, respectively, with a load resistance of 101 MΩ (Figure S7). The current amplitude decreases with an increase in load resistance, while the voltage rises up conversely. As a result, the peak power density achieves 9.68 W/m^2 at a load

DOI: 10.1021/am507477y
ACS Appl. Mater. Interfaces 2015, 7, 1275–1283

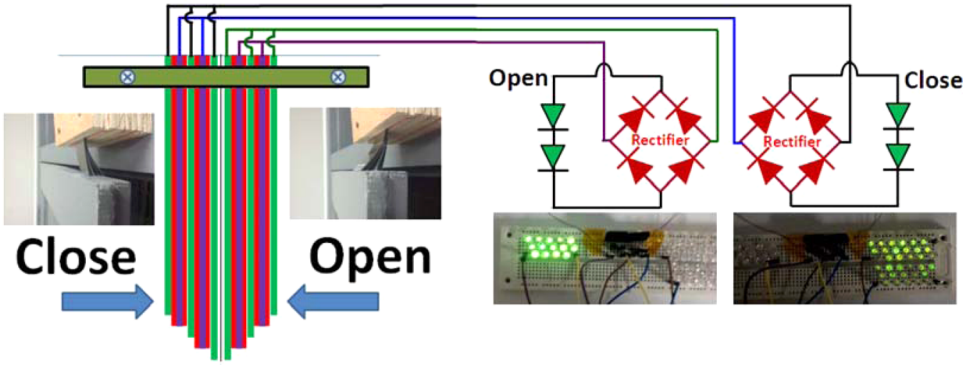

Figure 7. Structure diagram of the self-power door monitor. The four insets are the digital photographs of the corresponding states and its lit LEDs.

resistance of 5 MΩ as is displayed in Figure 6b. In comparison with the previous triboelectric nanogenerators, the NTEG's performance is greatly enhanced with a greater output current and a higher power density. It demonstrates great advantages of the generators using elastic potential to enhance its energy conversion efficiency.

3.3. Practical Applications. *3.3.1. Powering Commercial LEDs.* To test the capacity of NTEG as a power source, we use the 11-slice NTEG to drive commercial LEDs directly, as displayed in Figure 6c, in which we can see that the output current can reach as high as 205 μA. Two rows of LEDs connected in series are lit up simultaneously, as can be seen in the inset. The bright light of these LEDs implies the high energy density output of the NTEG.

3.3.2. Charging Commercial Capacitors. When the NTEG harvests the energy from moving objects, it could produce high pulse currents. Therefore, we cannot use the high output voltage and alternating current pulses to directly power electric devices in many cases, as those devices often need a constant and low bias. Storage units such as a supercapacitor,[31] capacitor,[32,33] or battery can store the pulse energy and later provides a supply of regulated power. Here, we choose a commercial capacitor (47 μF) for energy storage which is charged by the 11-slice NTEG with an active length of 6 cm at a frequency of 2.5 Hz. As shown in Figure 6d, it demonstrates the charging voltage−time signals of the capacitor connected with two LEDs, from which we can observe that the capacitor is charged from 0 to 4.2 V within 30 s and simultaneously powers the two LEDs. The lower inset depicts the equivalent circuit loop and the upper inset is the enlarged plot of the voltage curve, where the stepped increase in the voltage corresponds to the separation and contact of the electrodes. The two digital photographs in Figure 6d exhibit the two LEDs in charging state.

3.3.3. Application of a Self-powered Door Monitor System. Harvesting energy of different forms is of great importance for triboelectric generators, which is featured by harvesting energy from ambient environment, such as the motion of doors, the rotation of taps, and the drawing of drawers. The NTEG can harvest not only the mechanical energy from fan blade rotating but also from translation motion and vibration. To testify this capacity, a frequently opened and closed door is chosen as the power source, as it has the features of translation motion and vibration. The NTEG is successfully applied to door monitor, which works by monitoring the states of doors in real time. In the experiment, we put two NTEGs back to back with PVC in the middle as the insulated material to prevent the NTEGs from affecting each other. NTEGs are fixed on the doorframe, with the door as a blade hitting the slices back and forth. As shown in Figure 7, the wires connect two NTEGs to the door monitor circuit. When the door is opened or closed, it hits the corresponding NTEG, generating respective currents, which light up the corresponding LEDs after rectification. The photographs show the working state of a real NTEG in the inset in Figure 7, from which we can observe that the LEDs of door monitor work without any external power supply. The whole harvesting process demonstrates that the NTEG can convert the energy of the movement of a door to electrical energy without affecting the regular use of the door.

Based on the investigations of the output performance of the NTEG in different conditions, the NTEG has great potential application in harvesting energy of different forms from the ambient environment to drive a self-powered system.

4. CONCLUSIONS

A notepad-like triboelectric generator has been designed and fabricated which can achieve high current output under low-velocity motion by utilizing spring lamination. The elastic potential energy is employed to efficiently convert low-velocity motion to high-velocity motion to improve electromechanical conversion efficiency. The notepad-like structure design enables the generator to harvest energy from rotation, translation, and vibration from the ambient environment. The working mechanism is discussed in detail. In addition, the factors that may affect the output performance have been investigated by changing the related parameters including the number of slices, active length, applied frequency, and press displacement. Through these experiments, the maximum short-circuit current, open-circuit voltage, and power density are achieved to be 205 μA, 470 V, and 9.68 W/m^2, respectively. Compared with the previous triboelectric nanogenerators, the NTEG's performance is greatly enhanced with a greater output current and a higher power density due to its high electromechanical conversion efficiency. The NTEG can be used to light up more than 200 LEDs, to charge capacitors to 4.2 V in 30 s, and to apply to a self-powered door monitor. The NTEG is flexible, light, durable, cost-effective, and portable. Therefore, we can see that this NTEG has great potential in smart home sensing, environmental monitoring, and personal electronics.

DOI: 10.1021/am507477y
ACS Appl. Mater. Interfaces 2015, 7, 1275−1283

■ ASSOCIATED CONTENT

Supporting Information

Figures S1−S7 as mentioned in the text. Calculation of the power density. This material is available free of charge via the Internet at http://pubs.acs.org.

■ AUTHOR INFORMATION

Corresponding Author

*Tel.: +86 23 65678362. Fax: +86 23 65678362. E-mail address: hucg@cqu.edu.cn.

Notes

The authors declare no competing financial interest.

■ ACKNOWLEDGMENTS

This work is supported by the NSFCQ (cstc2012jjB0006), the National High Technology Research and Development Program of China (SQ2015AA0302342), SRFDP (20110191110034, 20120191120039), NSFC (11204388), and the Fundamental Research Funds for the Central Universities (CDJRC10300001, CDJZR11300004, CDJZR12225501, and CQDXWL-2013-012).

■ REFERENCES

(1) Wang, Z. L.; Song, J. H. Piezoelectric Nanogenerators Based on Zinc Oxide Nanowire Arrays. *Science* **2006**, *312*, 242−246.

(2) Wang, Z. L.; Zhu, G.; Yang, Y.; Wang, S.; Pan, C. Progress in Nanogenerators for Portable Electronics. *Mater. Today* **2012**, *15*, 532−543.

(3) Mitcheson, P. D.; Yeatman, E. M.; Rao, G. K.; Holmes, A. S.; Green, T. C. Energy Harvesting from Human and Machine Motion for Wireless Electronic Devices. *Proc. IEEE* **2008**, *96*, 1457−1486.

(4) Chang, C.; Tran, V. H.; Wang, J.; Fuh, Y.-K.; Lin, L. Direct-Write Piezoelectric Polymeric Nanogenerator with High Energy Conversion Efficiency. *Nano Lett.* **2010**, *10*, 726−731.

(5) Chen, X.; Xu, S.; Yao, N.; Shi, Y. 1.6 V Nanogenerator for Mechanical Energy Harvesting Using PZT Nanofibers. *Nano Lett.* **2010**, *10*, 2133−2137.

(6) Lee, K. Y.; Bae, J.; Kim, S.; Lee, J.-H.; Yoon, G. C.; Gupta, M. K.; Kim, S.; Kim, H.; Park, J.; Kim, S.-W. Depletion Width Engineering via Surface Modification for High Performance Semiconducting Piezoelectric Nanogenerators. *Nano Energy* **2014**, *8*, 165−173.

(7) Heremans, J. P.; Jovovic, V.; Toberer, E. S.; Saramat, A.; Kurosaki, K.; Charoenphakdee, A.; Yamanaka, S.; Snyder, G. J. Enhancement of Thermoelectric Efficiency in PbTe by Distortion of the Electronic Density of States. *Science* **2008**, *321*, 554−557.

(8) Leng, Q.; Chen, L.; Guo, H.; Liu, J.; Liu, G.; Hu, C.; Xi, Y. Harvesting Heat Energy from Hot/Cold Water with a Pyroelectric Generator. *J. Mater. Chem. A* **2014**, *2*, 11940−11947.

(9) Lee, J.-H.; Lee, K. Y.; Gupta, M. K.; Kim, T. Y.; Lee, D.-Y.; Oh, J.; Ryu, C.; Yoo, W. J.; Kang, C. Y.; Yoon, S.-J.; Yoo, J. B.; Kim, S. W. Highly Stretchable Piezoelectric-Pyroelectric Hybrid Nanogenerator. *Adv. Mater.* **2014**, *26*, 765−769.

(10) Fan, F.-R.; Tian, Z.-Q.; Wang, Z. L. Flexible Triboelectric Generator. *Nano Energy* **2012**, *1* (2), 328−334.

(11) Wang, S.; Lin, L.; Wang, Z. L. Nanoscale Triboelectric-Effect-Enabled Energy Conversion for Sustainably Powering Portable Electronics. *Nano Lett.* **2012**, *12* (12), 6339−6346.

(12) Niu, S.; Zhou, Y. S.; Wang, S.; Liu, Y.; Lin, L.; Bando, Y.; Wang, Z. L. Simulation Method for Optimizing the Performance of an Integrated Triboelectric Nanogenerator Energy Harvesting System. *Nano Energy* **2014**, *8*, 150−156.

(13) Xie, Y.; Wang, S.; Lin, L.; Jing, Q.; Lin, Z.-H.; Niu, S.; Wu, Z.; Wang, Z. L. Rotary Triboelectric Nanogenerator Based on a Hybridized Mechanism for Harvesting Wind Energy. *ACS Nano* **2013**, *7* (8), 7119−7125.

(14) Guo, H.; He, X.; Zhong, J.; Zhong, Q.; Leng, Q.; Hu, C.; Chen, J.; Tian, L.; Xi, Y.; Zhou, J. A Nanogenerator for Harvesting Airflow Energy and Light Energy. *J. Mater. Chem. A* **2014**, *2*, 2079−2087.

(15) Zhu, G.; Chen, J.; Zhang, T.; Jing, Q.; Wang, Z. L. Radial-Arrayed Rotary Electrification for High Performance Triboelectric Generator. *Nat. Commun.* **2014**, *5*, 3426 DOI: 10.1038/ncomms4426.

(16) Lin, Z. H.; Cheng, G.; Wu, W. Z.; Pradel, K. C.; Wang, Z. L. Dual-Mode Triboelectric Nanogenerator for Harvesting Water Energy and as a Self-Powered Ethanol Nanosensor. *ACS Nano* **2014**, *8*, 6440−6448.

(17) Yu, A.; Jiang, P.; Wang, Z. L. Nanogenerator as Self-Powered Vibration Sensor. *Nano Energy* **2012**, *1* (3), 418−423.

(18) Chen, J.; Zhu, G.; Yang, W.; Jing, Q.; Bai, P.; Yang, Y.; Hou, T.-C.; Wang, Z. L. Harmonic-Resonator-Based Triboelectric Nanogenerator as a Sustainable Power Source and a Self-Powered Active Vibration Sensor. *Adv. Mater.* **2013**, *25* (42), 6094−6099.

(19) Jing, Q.; Zhu, G.; Bai, P.; Xie, Y.; Chen, J.; Han, R. P. S.; Wang, Z. L. Case-Encapsulated Triboelectric Nanogenerator for Harvesting Energy from Reciprocating Sliding Motion. *ACS Nano* **2014**, *8*, 3836−3842.

(20) Guo, H.; Leng, Q.; He, X. M.; Wang, M. J.; Chen, J.; Hu, C. G.; Xi, Y. A Triboelectric Generator Based on Checker-Like Interdigital Electrodes with a Sandwiched PET Thin Film for Harvesting Sliding Energy in All Directions. *Adv. Energy Mater.* **2014**, DOI: 10.1002/aenm.201400790.

(21) Lin, L.; Wang, S.; Xie, Y.; Jing, Q.; Niu, S.; Hu, Y.; Wang, Z. L. Segmentally Structured Disk Triboelectric Nanogenerator for Harvesting Rotational Mechanical Energy. *Nano Lett.* **2013**, *13* (6), 2916−2923.

(22) Zhang, X.-S.; Han, M.-D.; Wang, R.-X.; Meng, B.; Zhu, F.-Y.; Sun, X.-M.; Hu, W.; Wang, W.; Li, Z.-H.; Zhang, H.-X. High-Performance Triboelectric Nanogenerator with Enhanced Energy Density Based on Single-Step Fluorocarbon Plasma Treatment. *Nano Energy* **2014**, *4*, 123−131.

(23) Guo, H.; Leng, Q.; Xi, Y.; Chen, J.; Wang, M. J.; He, X. M.; Hu, C. G. Spiral-Interdigital-Electrode-Based Multifunctional Device: Dual-Functional Triboelectric Generator and Dual-Functional Self-Powered Sensor. *Nano Energy* **2014**, DOI: 10.1016/j.nanoen.2014.09.021.

(24) Yang, J.; Chen, J.; Liu, Y.; Yang, W.; Su, Y.; Wang, Z. L. Triboelectrification-Based Organic Film Nanogenerator for Acoustic Energy Harvesting and Self-Powered Active Acoustic Sensing. *ACS Nano* **2014**, *8*, 2649−2657.

(25) Yang, Y.; Zhang, H.; Lin, Z.-H.; Zhou, Y. S.; Jing, Q.; Su, Y.; Yang, J.; Chen, J.; Hu, C.; Wang, Z. L. Human Skin Based Triboelectric Nanogenerators for Harvesting Biomechanical Energy and as Self-Powered Active Tactile Sensor System. *ACS Nano* **2013**, *7*, 9213−9222.

(26) Zheng, Q.; Shi, B.; Fan, F.; Wang, X.; Yan, L.; Yuan, W.; Wang, S.; Liu, H.; Li, Z.; Wang, Z. L. In Vivo Powering of Pacemaker by Breathing-Driven Implanted Triboelectric Nanogenerator. *Adv. Mater.* **2014**, *26*, 5851−5856.

(27) Boland, J.; Chao, Y. H.; Suzuki, Y.; Tai, Y. C.; Ieee, I. Micro Electret Power Generator. In *Proceedings of the 16th IEEE International Conference on Micro Electro Mechanical Systems*, Kyoto, Japan, Jan. 23, 2003; p 538.

(28) Xie, Y.; Wang, S.; Lin, L.; Jing, Q.; Lin, Z.-H.; Niu, S.; Wu, Z.; Wang, Z. L. Rotary Triboelectric Nanogenerator Based on a Hybridized Mechanism for Harvesting Wind Energy. *ACS Nano* **2013**, *7*, 7119−7125.

(29) Zhu, G.; Pan, C.; Guo, W.; Chen, C.-Y.; Zhou, Y.; Yu, R.; Wang, Z. L. Triboelectric-Generator-Driven Pulse Electrodeposition for Micropatterning. *Nano Lett.* **2012**, *12*, 4960−4965.

(30) Zhu, G.; Lin, Z.-H.; Jing, Q.; Bai, P.; Pan, C.; Yang, Y.; Zhou, Y.; Wang, Z. L. Toward Large-Scale Energy Harvesting by a Nanoparticle-Enhanced Triboelectric Nanogenerator. *Nano Lett.* **2013**, *13*, 847−853.

(31) Wang, G.; Zhang, L.; Zhang, J. A Review of Electrode Materials for Electrochemical Supercapacitors. *Chem. Soc. Rev.* **2012**, *41*, 797−828.

DOI: 10.1021/am507477y
ACS Appl. Mater. Interfaces 2015, 7, 1275−1283

(32) Yu, G.; Xie, X.; Pan, L.; Bao, Z.; Cui, Y. Hybrid Nanostructured Materials for High-Performance Electrochemical Capacitors. *Nano Energy* **2013**, *2* (2), 213−234.
(33) Hu, L.; Zheng, G.; Yao, J.; Liu, N.; Weil, B.; Eskilsson, M.; Karabulut, E.; Ruan, Z.; Fan, S.; Bloking, J. T.; McGehee, M. D.; Wagberg, L.; Cui, Y. Transparent and Conductive Paper from Nanocellulose Fibers. *Energy Environ. Sci.* **2013**, *6*, 513−518.

DOI: 10.1021/am507477y
ACS Appl. Mater. Interfaces 2015, 7, 1275−1283